Radiotherapy and Oncology 134 (2019) 101–109

Contents lists available at ScienceDirect

Radiotherapy and Oncology

journal homepage: www.thegreenjournal.com

Original Article

Effect of setup and inter-fraction anatomical changes on the accumulated dose in CT-guided breath-hold intensity modulated proton therapy of liver malignancies

Zhiyong Yang [a,b], Yu Chang [a], Kristy K. Brock [c], Guillaume Cazoulat [c], Eugene J. Koay [d], Albert C. Koong [d], Joseph M. Herman [d], Peter C. Park [b], Falk Poenisch [b], Qin Li [a], Kunyu Yang [a], Gang Wu [a], Brian Anderson [c], Andrea N. Ohrt [c], Yupeng Li [b], X. Ronald Zhu [b], Xiaodong Zhang [b], Heng Li [b,*]

[a] Cancer Center, Union Hospital, Tongji Medical College, Huazhong University of Science and Technology, Wuhan, China; [b] Department of Radiation Physics, The University of Texas MD Anderson Cancer Center; [c] Department of Image Physics, The University of Texas MD Anderson Cancer Center; and [d] Division of Radiation Oncology, The University of Texas MD Anderson Cancer Center, Houston, United States

ARTICLE INFO

Article history:
Received 26 July 2018
Received in revised form 4 December 2018
Accepted 22 January 2019
Available online 6 February 2019

Keywords:
Accumulated dose
Liver cancer
Intensity-modulated proton therapy

ABSTRACT

Purpose: To evaluate the effect of setup uncertainties including uncertainties between different breath holds (BH) and inter-fractional anatomical changes under CT-guided BH with intensity-modulated proton therapy (IMPT) in patients with liver cancer.

Methods and materials: This retrospective study considered 17 patients with liver tumors who underwent feedback-guided BH (FGBH) IMRT treatment with daily CT-on-rail imaging. Planning CT images were acquired at simulation using FGBH, and FGBH CT-on-rail images were also acquired prior to each treatment. Selective robust IMPT plans were generated using planning CT and re-calculated on each daily CT-on-rail image. Subsequently, the fractional doses were deformed and accumulated onto the planning CT according to the deformable image registration between daily and planning CTs. The doses to the target and organs at risk (OARs) were compared between IMRT, planned IMPT, and accumulated IMPT doses.

Results: For IMPT plans, the mean of $D_{98\%}$ of CTV for all 17 patients was slightly reduced from the planned dose of 68.90 ± 1.61 Gy to 66.48 ± 1.67 Gy for the accumulated dose. The target coverage could be further improved by adjusting planning techniques. The dose–volume histograms of both planned and accumulated IMPT doses showed better sparing of OARs than that of the IMRT.

Conclusions: IMPT with FGBH and CT-on-rail guidance is a robust treatment approach for liver tumor cases.

© 2019 Elsevier B.V. All rights reserved. Radiotherapy and Oncology 134 (2019) 101–109

Liver cancer is one of the most common causes of cancer-related deaths [1,2]. Radiotherapy for liver cancer is difficult because of the low tolerance of the liver to radiation, sparing of adjacent normal structures, respiratory motion, and challenges in localizing the intrahepatic target during radiotherapy [3–6]. Compared with radiotherapy with photons, e.g., intensity-modulated photon therapy (IMRT), proton therapy is characterized by a sharp dose fall-off around the target volume. Therefore, proton therapy can deliver a higher dose to liver tumor while preserving much more normal liver tissue than IMRT [1]. This is especially important in patients with compromised liver function such as advanced cirrhosis in patients with hepatocellular carcinoma or steatohepatitis due to extensive chemotherapy.

During radiotherapy, liver tumors show considerable movement due to respiration and changes in gastrointestinal (GI) filling [5,7–9]. Various approaches have been developed to actively manage respiratory motion during IMRT, including abdominal compression [6,10], tumor/fiducial tracking [11–13], gating during normal respiration [4], and breath hold (BH) [14]. Because the proton beam has a finite range, when anatomical variations occur in between the acquisition of the planning CT and the subsequent treatment fractions, the dose distributions will be changed and result in undershooting or overshooting. Hence, BH is a desirable option in proton therapy for a number of reasons, e.g., minimization of tumor motion, maximization of separation between the gross tumor volume (GTV) and adjacent organs at risk (OARs), reduction of delivery time compared with free-breathing gating, and the ability to perform volumetric verification imaging [15]. However, the reproducibility of the BH in different treatment techniques has not been validated. Inter-fractionally, the BH

* Corresponding author at: Department of Radiation Physics, The University of Texas MD Anderson Cancer Center, 1840 Old Spanish Trail, Houston, TX, USA.
E-mail address: hengli@mdanderson.org (H. Li).

https://doi.org/10.1016/j.radonc.2019.01.028
0167-8140/© 2019 Elsevier B.V. All rights reserved.

uncertainties, or the difference in BH levels between different BHs, albeit small, could potentially lead to large changes in the proton beam range and patient dose distribution; whereas intra-fractionally, excessive residual respiratory motion within the same BH could also contribute to dosimetric uncertainties.

Various strategies have also been proposed for proton therapy, and some have been implemented: water equivalent thickness (WET)-guided beam angle selection and rescanning strategy, which can cope with intra-fractional anatomical changes [16–18]; robustness optimization which accounts for setup and range uncertainties, could also reduce the impact of anatomical changes [19]; and 4D robustness and multi-CT optimization, which can include setup and range uncertainties as well inter-fractional anatomical changes but sacrifices some adjacent OARs [20,21].

To address these uncertainties, in this study we hypothesize that robust optimized intensity-modulated proton therapy (IMPT) could minimize the effect of BH uncertainties. This is based on the observation that the BH uncertainties could be approximated as an isocenter shift with major axis on the superior-inferior (SI) direction, which is taken into consideration explicitly in the robust optimization process. Furthermore, we also used WET guided beam angle selection to reduce the sensitivity of IMPT plan toward residual motion. Since patients treated with FGBH in general have small residual motion during the beam-on gating window, we considered the interplay effect due to the residual motion to be small. By choosing field angles that were affected by possible respiratory motion the least, we could further reduce the dosimetric effect of residual motion.

The purpose of this study was to investigate the effect of setup and inter-fractional anatomical changes (e.g., BH uncertainties, liver and GI tract deformation) in liver cancer patients on the accumulated fractional doses when using IMPT. We retrospectively analyzed seventeen patients who had CT-on-rail images acquired prior to daily treatment for 10–15 fractions. IMPT plans were generated using the selective robust optimization technique on the planning CT and re-calculated on CT-on-rail images to test and verify the reproducibility of FGBH, the inter-fraction liver deformations, and the effects to the accumulated IMPT dose distributions.

Methods and materials

Patient information and simulation

Seventeen patients with liver tumors treated with FGBH between September 2017 and January 2018 were selected for this retrospective study. All patients in this study were enrolled in an institutional review board-approved retrospective data collection protocol. Table 1 summarizes the characteristics (e.g., sex, tumor type, and weight) of these patients. Each patient had completed IMRT treatment with at least 10 fractions on a previously described integrated CT/LINAC system [5,24].

Patients were immobilized using a large hemi-body vacuum bag (BlueBAG; Elekta Co., Atlanta, GA, USA) with arms above their heads, using a wing board and a T-bar (Extended Wing Board; CIVCO, Kalona, IA, USA). A 4DCT was first acquired to evaluate tumor motion when patient breathe normally. The patient would then be instructed to take a breath and hold the position, and FGBH CT scans were acquired. 3–5 FGBH CTs would be acquired, each within a BH, to test the intra-fraction BH reproducibility. The BH beam-on window size was set to 3 mm for the external surrogate motion, to ensure a small residual motion. The procedures for using the Varian RPM system (Varian Medical Systems, Palo Alto, CA, USA) with feedback both for monitoring the BH and for guiding the patient in maintaining a consistent BH level have been described extensively in the literature [25]. The T0 phase, which represents the end-of-inspiration of 4DCT, and FGBH CT data sets were transferred to the Eclipse system (Varian Medical Systems, Palo Alto, CA, USA) for treatment planning.

IMRT planning and treatment delivery

FGBH CT was used as the reference CT for IMRT planning. GTV was contoured and expanded by 8 mm for subclinical disease to obtain the clinical target volume (CTV) (clinical target volume plus internal margin). Then CTV was expanded by 3 mm for setup uncertainties (BH uncertainties included), to obtain a planning target volume (PTV). All OARs were also contoured on FGBH CT. IMRT plans were prescribed to 67.5 Gy in 15 fractions, using 7 to 11 6-MV photon fields. The normalization point was CTV $D_{99\%}$ of 67.5 Gy, where $D_{x\%}$ is defined as the lowest dose covering x% of the volume. The PTV was covered with an isodose line above 80% of the prescription dose. All these IMRT plans had been clinically approved, and all treatments had been completed. Since not all patients complete all their treatments on the CT/Linac system, daily CT data set for several of the patients were not complete.

All patients were treated with the CT/LINAC system using the same FGBH system as in the simulation. Patients were placed in the immobilization device and aligned to the skin marks placed at simulation. Before treatment, patients underwent CT scanning with FGBH, to verify BH and setup reproducibility. The same CT imaging protocol was used for simulation and daily CTs. Each patient was aligned first based on bony anatomy (a section of the spine at the level of the GTV) and secondly on the tumor's location with respect to the contoured GTV location. If the GTV position with respect to bony anatomy was consistent, the patient was treated at that location. Otherwise, the patient was aligned so that the tumor was covered by the contoured GTV, but this situation was rare. Two patients have been implanted fiducial markers which could also be a reference for the tumor position. The registration and alignment results were recorded for retrospective analysis. Detailed procedures for treatment delivery have been described before [25]. Once the CT image alignment was approved by the attending physician, the fields were delivered under repeated FGBHs, generally 1–2 FGBHs per field. The entire process from patient setup to the end of treatment generally took about 30 min.

IMPT planning

Because the end-of-inspiration phase (CT0) of 4DCT is the phase nearest to the breath hold of inspiration, we calculated the WET from the beam entrance on body surface to voxels in the CTV on a beam direction both on the CT0 and FGBH CT sets to evaluate the possible effect of residual motion. The ΔWET is the mean value of the WET differences between CT0 and FGBH for all voxels within the CTV. The ΔWET was calculated for 180° ranges on the patient's right side (liver side) at increments of 5° to yield a patient-specific ΔWET curve as a function of beam angle. A larger ΔWET indicates that the proton beam from the particular angle is sensitive to respiratory motion and residual motion within the BH window [16]. For IMPT planning, 3 or 4 beam angles were chosen from the minimum values of ΔWET. We used this method to avoid large anatomical variances from the intra-fractional residual motion.

FGBH CT and contours as described above were used for IMPT treatment planning. IMPT plans were optimized with multi-field optimization technique using the Eclipse v13.7 treatment planning system. To account for the setup and range uncertainties the selective robustness optimization was applied [26]. The objective function of CTV was computed for worst-case situations, using assigned perturbations including range uncertainties of ±3.5% and isocenter shifts of ±3 mm. Since in the robust optimization process both setup uncertainties and BH uncertainties could be modeled by iso-center shifts on cardinal directions, the two could be combined

Table 1
Patient and target characteristics.

Patient	Weight before treatment (kg)	Weight after treatment (kg)	Sex	Tumor type	Number of available CTs	CTV volume (cm^3)
1	65.8	63.0	Male	Hepatocellular carcinoma	10[a]	165.1
2	96.7	96.7	Male	Metastatic liver disease	15	89.6
3	81.8	81.8	Male	Metastatic liver disease	12[a]	433.9
4	91.8	87.1	Male	Hepatocellular carcinoma	15	520.0
5	65.3	62.8	Male	Cholangiocarcinoma	15	132.9
6	91.1	86.2	Male	Hepatocellular carcinoma	15	638.5
7	54.7	55.7	Female	Metastatic liver disease	10[a]	31.0
8	77.0	77.0	Female	Hepatocellular carcinoma	15	686.5
9	87.7	79.7	Female	Metastatic liver disease	15	1137.4
10	77.4	75.5	Male	Cholangiocarcinoma	15	566.3
11	63.8	64.1	Male	Cholangiocarcinoma	15	177.9
12	81.2	81.5	Male	Metastatic liver disease	10[a]	12.9
13	56.1	55.9	Female	Cholangiocarcinoma	10[a]	42.0
14	106.5	102.8	Male	Hepatocellular carcinoma	11[a]	185.0
15	57.8	57.9	Male	Hepatocellular carcinoma	15	763.4
16	56.6	57.5	Female	Cholangiocarcinoma	15	29.4
17	82.6	83.5	Female	Cholangiocarcinoma	15	133.6

Abbreviations: CTV = clinical target volume.
[a] The missing fractions of CT-on-rail images were replaced by planning CTs.

in assigning the isocenter shifts for the worst-case scenario. Previous studies suggested that the overall precision for the CT/Linac system for rigid setups to be within 1 mm [24], whereas the BH uncertainties to be ~2 mm with FGBH [25]. Therefore the total isocenter shifts were assigned to ±3 mm. The optimization objective for all plans was to achieve full coverage of the prescribed dose to the CTV and to minimize the dose to OARs, and the normalization point was set to CTV $D_{99.99\%}$ of 67.5 Gy relative biological effectiveness (RBE).

IMPT delivery

The beam delivery system (PROBEAT; Hitachi America, Ltd., Tarrytown, NY) used at University of Texas MD Anderson Cancer Center provides discrete spot scanning using a synchrotron [22,23]. The dose rate of the system is 100 s to deliver 2 Gy to a $10 \times 10 \times 10\ cm^3$ volume in a water phantom with most distal point in the volume at 30 g/cm^2 depth. The time required per spot irradiation (irradiation time + travel time) ranges from 1 to 10 ms, depending on spot monitor units (MU). The scanning velocity is 12 m/s for a depth of 10.7 g/cm^2 and 9 m/s for a depth of 30 g/cm^2. The synchrotron generates a spill of proton beams with the maximum duration of 4.4 s in each acceleration cycle. Switching of energy requires a new spill. Deceleration and acceleration of protons between spills take 2.1 s.

Plan evaluation and comparison

Before calculation of the accumulated dose on the daily CT-on-rail images, the CT-on-rail images were first non-rigidly registered to the planning CT images. MORFEUS, a biomechanical deformable registration algorithm in RayStation (MORFEUS v0.9, RayStation v4.6, RaySearch Laboratories, Stockholm, Sweden) was used in this study for deformable image registration, since its accuracy has been evaluated in previous studies [27–29]. The MORFEUS was also used to automatically propagate all contours (includes targets and OARs) from the planning CT to all CT-on-rail daily CTs, and the propagated contours on daily CTs were visually verified. The IMPT plan was re-calculated on the CT-on-rail daily CTs with iso-center aligned by the registration results performed at the time of treatment for all fractions treated on the CT/Linac unit. The deformed daily doses were then accumulated onto the planning CT using the deformable image registration vectors.

To quantify the differences between dose distributions, we used dose-volume histograms to assess the dose coverage of the CTV and the protection of OARs. The CTV evaluation parameters were $D_{98\%}$, $D_{2\%}$, the conformity index (CI), and the homogeneity index (HI). The CI ($CI = 100\% \times [TV_{PI}]^2/[PI_{100} \times TV]$) describes the conformity of the prescribed dose around the target volume [30]. TV is the target volume, TV_{PI} is the volume of the target covered by the prescribed isodose, and PI_{100} is the volume receiving 100% of the prescribed isodose; conformity is better as the index approaches 100%. The HI ($HI = 100\% \times (D_{2\%} - D_{98\%})/D_{50\%}$) is used to document dose heterogeneity within each target volume; plans that are more homogenous have values closer to 0% [31]. Mean dose (D_{mean}) and the volume that received 40 Gy (V40) to the parallel OARs (e.g., duodenum) were compared. For the spinal cord, the maximum doses were compared. For the liver, D_{mean} and the volume that received 5 Gy (V5) to the normal liver tissues (liver-GTV) were evaluated.

To evaluate the dosimetry advantage of the IMPT plans, we re-normalized the accumulated IMPT plans to achieve the same dose indices of the adjunct OARs (D_{mean} for the liver, or V40, V60 or D_{mean} for the duodenum) of the IMRT plans. The boost IMPT plans were also evaluated and compared with the IMRT plans.

Statistical analysis

SPSS 24.0 software (IBM, Armonk, NY) was used for statistical analyses of all dosimetric indices. We used a paired, 2-tailed Wilcoxon signed-rank test to compare the dose distributions between 1) IMRT and planned IMPT, 2) IMRT and accumulated IMPT, 3) planned and accumulated IMPT, and 4) IMRT and boost IMPT. Comparisons 1 and 2 allowed us to evaluate the dosimetric advantages of these plans. Comparison 3 allowed us to assess the IMPT dose distribution changes to the inter-fraction BH uncertainties and anatomical variances. Comparison 4 allowed us to evaluate the maximum dosimetric advantages of the IMPT to IMRT plans. *P* values of less than 0.05 were considered statistically significant.

Results

Fig. 1 shows the CTV coverage of the 100% and 99% prescription doses of the accumulated IMPT doses for all 17 patients. All patients except patient 5 achieved at least 95% of CTV covered by 99% prescription line in the accumulated dose.

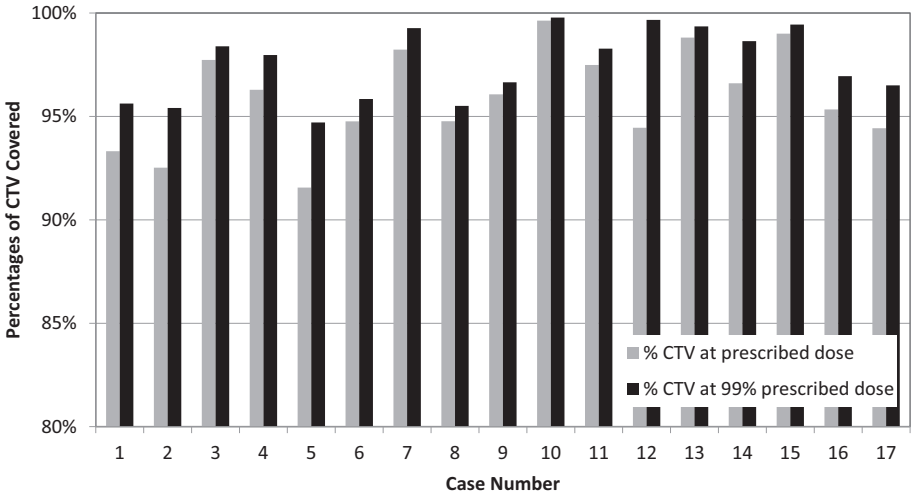

Fig. 1. Percentages of clinical target volume (CTV) receiving at least the prescribed dose (gray bars) and 99% of the prescribed dose (black bars) for the FGBH IMPT plans.

Table 2
Summary of analysis of target homogeneity (conformity) index and OARs.

Parameter	IMRT Dose	Planned IMPT Dose	Accumulated IMPT Dose	Boost IMPT Dose
CTV[a]				
$D_{98\%}$ (Gy)	68.43 (0.50)	68.90 (1.61)	66.48 (1.67)* +	75.89 (6.24)*
$D_{2\%}$ (Gy)	76.63 (6.63)	72.28 (1.42)*	71.97 (1.49)*	82.23 (7.17)*
HI (%)	0.11 (0.07)	0.05 (0.02)*	0.08 (0.01)+	0.08 (0.03)
CI (%)	0.82 (0.10)	0.70 (0.12)*	0.70 (0.13)*	–
Spinal cord[a]				
D_{max} (Gy)	18.61 (12.02)	6.51 (8.45)*	7.12 (9.75)*	8.04 (10.92)*
Liver-GTV[a]				
D_{mean} (Gy)	20.44 (6.37)	16.66 (5.69)*	17.35 (6.33)*	19.52 (6.68)
V5 (%)	75.82 (20.39)	45.07 (14.50)*	45.67 (19.20)*	48.31 (16.20)*
Duodenum[a]				
D_{mean} (Gy)	13.96 (14.49)	9.62 (10.82)*	10.25 (11.20)*	11.62 (12.79)
V40 (%)	14.17 (19.13)	7.61 (11.08)*	7.78 (11.45)*	10.42 (14.73)
Bowel[a]				
D_{mean} (Gy)	5.60 (7.11)	3.05 (5.44)*	3.06 (5.53)*	3.51 (6.39)
V40 (%)	2.52 (5.47)	2.02 (4.42)	1.81 (4.26)+	2.50 (5.76)
Stomach[a]				
D_{mean} (Gy)	12.25 (11.70)	3.30 (7.45)*	3.46 (7.42)*	3.98 (8.79)*
V40 (%)	8.48 (13.15)	2.77 (9.23)*	2.54 (9.21)*	3.25 (11.11)*
Right kidney[a]				
D_{mean} (Gy)	8.54 (13.15)	5.71 (8.06)*	5.69 (8.63)*	6.69 (9.24)
Left kidney[a]				
D_{mean} (Gy)	4.40 (5.09)	0.09 (0.28)*	0.15 (0.42)*	0.16 (0.46)*

Abbreviations: $D_{x\%}$ = dose delivered to x% of volume; HI = homogeneity index; CI = conformity index; Vy = percentage of volume receiving y Gy dose.
[a] Shown as mean (standard deviation).
* $P < 0.05$ compared to IMRT dose.
+ $P < 0.05$ for accumulated IMPT dose compared to planned IMPT dose.

Table 2 shows the CTV $D_{98\%}$, $D_{2\%}$, CI, and HI for IMRT, planned, accumulated, and boost IMPT doses. Between IMRT and IMPT plans with the same prescription, the IMRT plan had significant higher $D_{2\%}$ for CTV (Median (Range): 75.25 (5.92) Gy, Mean ± standard deviation (SD): 76.63 ± 6.63 Gy) than did the planned IMPT (Median (Range): 70.13 (3.41) Gy, Mean ± SD: 72.28 ± 1.42 Gy, $P = 0.001$) doses, and worse HI (Median (Range): 0.09 (0.29), Mean ± SD: 0.11 ± 0.07) for CTV than did the planned IMPT (Median (Range): 0.04 (0.04), Mean ± SD: 0.05 ± 0.02, $P = 0.001$) dose. However, the CI of IMRT plan (Median (Range): 0.86 (0.32), Mean ± SD: 0.82 ± 0.10) is better than the IMPT plans (Median (Range): 0.73 (0.48), Mean ± SD: 0.70 ± 0.12, $P = 0.002$). This could be due to the robust optimization process that considers the setup and range uncertainties and thus requires some high dose region surrounding the target.

The accumulated IMPT dose had lower $D_{98\%}$ (Median (Range): 66.81 (2.28) Gy, Mean ± SD: 66.48 ± 1.67 Gy) than did the IMRT (Median (Range): 68.63 (1.67) Gy, Mean ± SD: 68.43 ± 0.50 Gy, $P = 0.001$) and planned IMPT (Median (Range): 67.69 (0.84) Gy, Mean ± SD: 68.90 ± 1.61 Gy, $P = 0.003$) dose. However, with same OAR sparing, the boost accumulated IMPT dose had much higher $D_{98\%}$ (Median (Range): 76.55 (6.84) Gy, Mean ± SD: 75.89 ± 6.24 Gy) than did the IMRT (Median (Range): 68.63 (1.67) Gy, Mean ± SD: 68.43 ± 0.50 Gy, $P = 0.001$) dose.

OAR dose is also compared between the different plan doses in Table 2. Planned IMPT plans showed a significant decrease in all OARs such as those to the spinal cord (D_{max}(Mean ± SD) = 6.51 ± 8.45 Gy, $P < 0.001$) and normal liver tissues (liver-GTV) (D_{mean}(Mean ± SD) = 16.66 ± 5.69 Gy, $P < 0.001$) compared with

the IMRT plans. Accumulated IMPT plans also spared all the OARs, such as the spinal cord (D_{max} = 7.12 ± 9.75 Gy, $P < 0.001$) and normal liver tissues (D_{mean} = 17.35 ± 6.33 Gy, $P = 0.002$) much better than did the IMRT plans. Boost IMPT plans also achieve a better OAR sparing for the spinal cord (D_{max} = 8.04 ± 10.92 Gy, $P < 0.001$), normal liver tissues (V5(Mean ± SD) = 48.31 ± 16.20 %, $P < 0.001$), bowel (D_{mean} = 3.51 ± 6.39 Gy, $P = 0.028$), stomach (D_{mean} = 3.98 ± 8.79 Gy, $P = 0.001$), and left kidney (D_{mean} = 0.16 ± 0.46 Gy, $P = 0.001$) than did the IMRT plans. These results suggest that the IMPT plan could potentially deliver much higher dose to the target while spare OARs better than did the IMRT plan.

Planar dose and dose-volume histograms of planned IMPT and IMRT for case 10 are compared in Fig. 2. Fig. 2a and b shows the planar doses of planned IMPT and IMRT, respectively; the low dose area is much smaller in the IMPT plan than in the IMRT plan. Fig. 2c shows the differences between the planned IMPT (triangle line) and the IMRT (square line). The planned IMPT plan had a better CTV HI as well as a lower dose to all OARs than did the IMRT plan, e.g. V5 of the normal liver tissues (liver-GTV) in Fig. 2c.

Discussion

In this study, we found that the IMPT plan could achieve better sparing of OARs compared with the IMRT plan. The results also indicated that IMPT has the potential to further boost the target dose compared with IMRT. However, the accumulated dose coverage showed that the inter-fraction BH uncertainties and liver deformation impacted the IMPT plans of case 5. Previously, there has been limited information available on the dosimetric effect of the uncertainties induced by respiratory motion, gastrointestinal filling and intrahepatic deformation on target coverage in proton therapy to abdominal tumors [8,17,18,32], and this study helps understand the dosimetric impact of these factors.

With daily CT guidance, patient setup and breath hold levels are highly reproducible between different fractions, and the BH uncertainty does not seem to disrupt daily IMPT dose with robust optimization. However, we found that even though the inter-fraction BH reproducibility may be adequate, the anatomical changes of gastrointestinal filling or liver deformation may affect the target coverage [27], as seen for case #5 in Fig. 1. The anatomical change and the dosimetric impact are shown in Fig. 3c and d, which are the

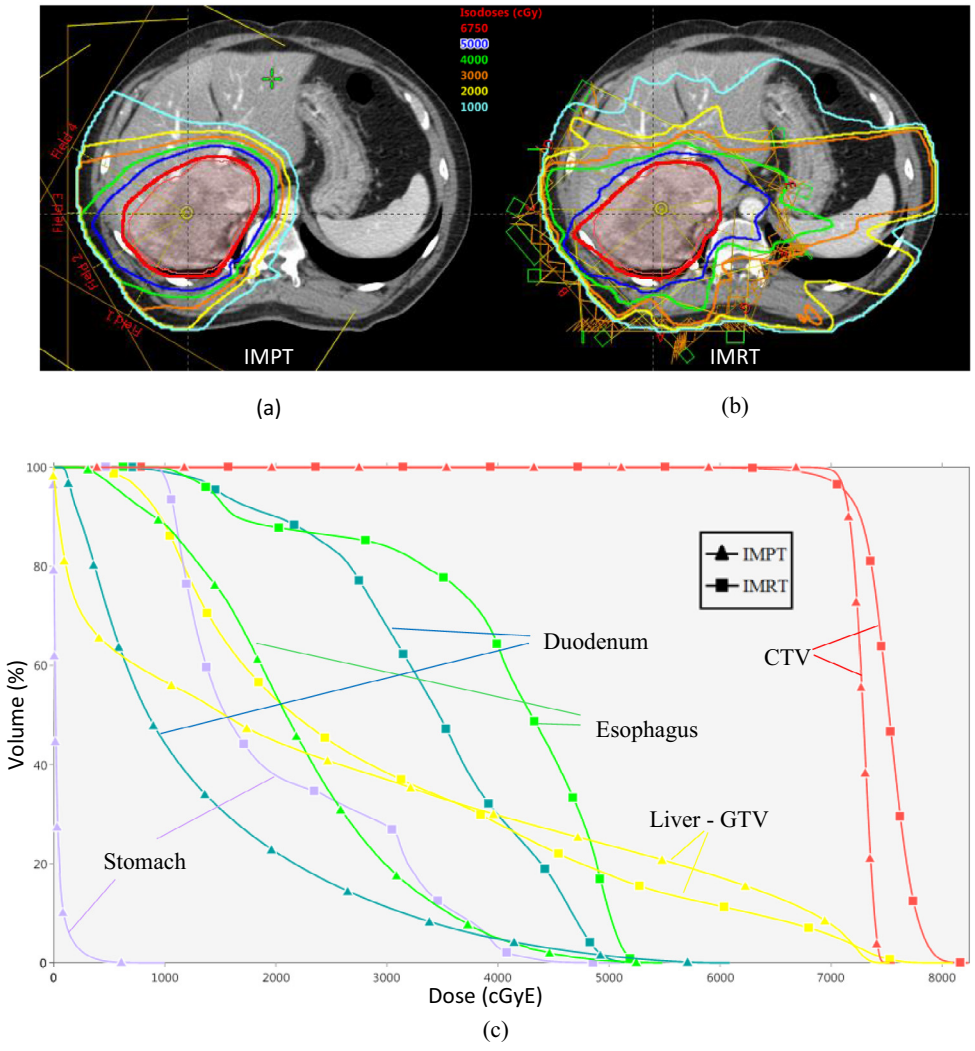

Fig. 2. Axial view of the same planar doses and fields for (a) the IMPT plan and (b) the IMRT plan. (c) Comparison of dose distribution histograms of the IMPT plan (triangle line) and the IMRT plan (square line).

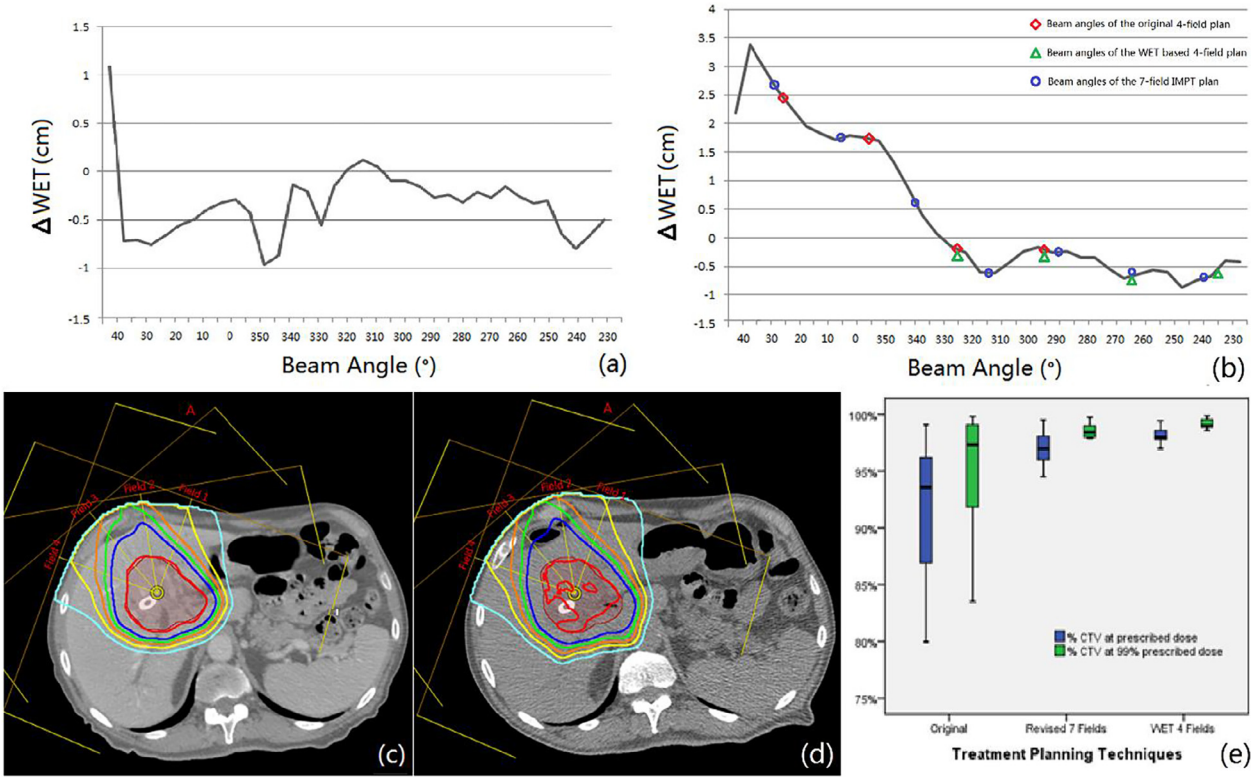

Fig. 3. (a) The ΔWET curve was created by plotting the ΔWET value between CT0 and BHCT for case #5 (b) The ΔWET curve was created by plotting the ΔWET value between the planning CT and the CT-on-rail images of the last fraction for case #5. The beam angles of the original IMPT plan, the revised 7 fields plan, and the WET based 4 fields plan were indicated with markers. The inter-fractional antimonial changes and the impact on IMPT dose distribution are shown in the axial view of the same planar images of (c) the planning CT and (d) the CT-on-rail images of the last fraction for the original IMPT plan. (e) Box plot of percentage CTV covered by prescribed dose and 99% of prescribed dose on dose re-calculated on daily CT for the original IMPT plan, the revised 7 fields plan, and the WET based 4 fields plan.

planned dose and the dose recalculated on the last daily CT, respectively. To find a strategy to account for the unpredictable inter-fraction BH uncertainties and anatomical changes, we re-planned and analyzed this case. For case #5, a patient with cholangiocarcinoma, the original 4-field IMPT plan has beam angles of 25°, 355°, 325°, 295°, which were chosen partly with WET analysis as shown in Fig. 3a. We again used the WET method, calculating the ΔWET between the planning CT and the last fraction CT-on-rail images. The larger ΔWET indicate the given beam angle could be impacted more by the anatomy change between the two CTs. The ΔWET was calculated from 45° to 235° at increments of 5°, and the result was shown in Fig. 3b. As shown in the figure, the larger differences occurred from 45° to 340°, which may be the result of gastrointestinal filling change or liver deformation, as also shown in Fig. 3c and 3d. The magnitude of WET change due to anatomy change is greater than the WET change due to respiratory motion for most beam angles. We tried 2 strategies to cope with these inter-fraction uncertainties. First, 4 beam angles of the minimum values of ΔWET (325°, 295°, 265°, and 235°) were chosen to re-optimize this plan; second, 7 evenly spread beam angles (30°, 5°, 340°, 315°, 290°, 265°, and 240°) were chosen to re-optimize this plan. The re-optimized results and dose–volume histograms of the planned dose, deform accumulated dose, and accumulated dose bands (variation ranges of the deformable dose of each fraction) are shown in Fig. 4. In addition, Fig. 3e shows the box plots for percentage of CTV volume covered by the prescription line and the 99% prescription line on daily dose distributions using the three different planning strategies. The WET based 4 fields plan had the best dose coverage of CTV and narrowest accumulated dose bands as shown in both Fig. 3e and Fig. 4. The 7-fields plan had better dose coverage of CTV and narrower accumulated dose bands than the origin IMPT. However, due to the increased liver volume irradiated, the liver doses were increased in both revised plans but still lower than the IMRT plan, while other OARs are similar for all three IMPT plans. In summary, the inter-fraction BH uncertainties and anatomical changes (e.g., gastrointestinal filling and/or intrahepatic deformation) were reduced in the revised plans. The CTV coverage of the 99% prescription dose was above 95% in both revised plans as shown in Fig. 3e. These results demonstrate that while IMPT is sensitive to uncertainties, robust IMPT plans could still be developed with advanced planning and imaging techniques.

Because the liver motion with the diaphragm during respiration can be controlled by the FGBH system, the day-to-day differences of intrahepatic deformation and filling of gastrointestinal organs are the greatest uncertainties that must be accounted for to ensure safe treatment. The left lobe of the liver is susceptible to deformation caused by stomach filing, whereas the right lobe is less affected by surrounding organs. Generally, we instruct our patients to ingest nothing for at least 3 hours before radiation treatment in an attempt to reduce the variability of stomach and bowel filling and enhance the tendency of the stomach and/or bowel to pull away from the left lobe of the liver. In this study, the weight variation of patients could be up to 10%, as shown in Table 1. However, patient weight change does not seem to be the key factor influencing the dose coverage of target, as no correlation between weight change and accumulated CTV coverage for the IMPT plans was found. Instead, the intrahepatic deformation in daily treatment may be an important factor influencing the dose coverage of target. In order to keep the plan robustness for the intrahepatic deformation uncertainties, we used the robust optimization to reduce the impact of intrahepatic deformation [19], and keep the plan

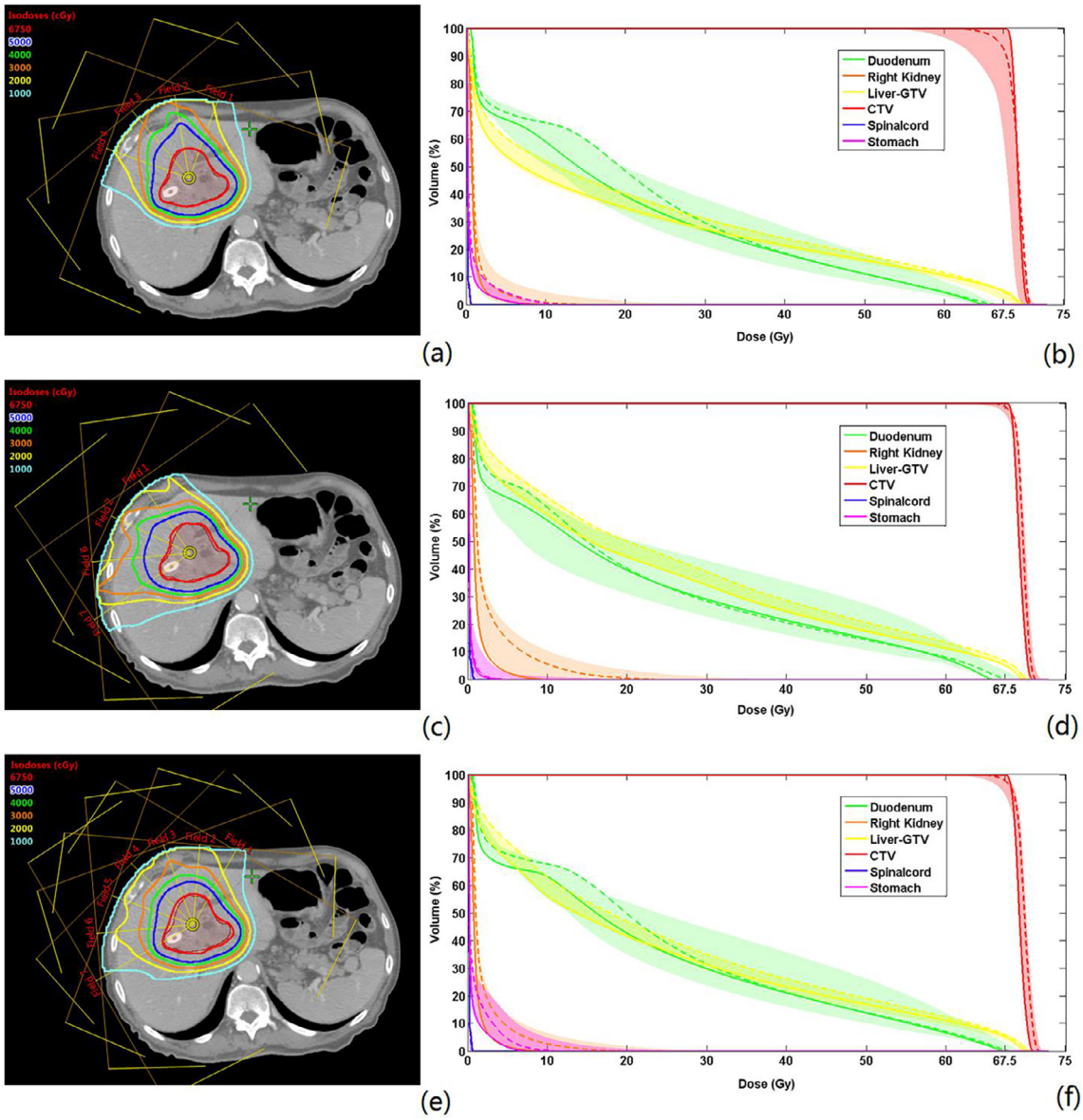

Fig. 4. The axial view of the same planar doses and fields of case #5 for (a) the original IMPT plan, (c) the IMPT plan with beam angles of the minimum values of ΔWET, and (e) the 7-field IMPT plan. The dose–volume histograms of the planned dose (solid line), the accumulated dose (dashed line), and the bands for all fractional doses of (b) the original IMPT plan, (d) the IMPT plan with beam angles of the minimum values of ΔWET, and (f) the 7-field IMPT plan.

robustness by normalizing the prescribed dose to full coverage of the target. The daily location of the tumor and plan isocenter alignments were also important, because the intrahepatic deformation may be hard to distinguish and the target may deform and move out of the fields. Although the daily CT or CBCT image-guided increases the total imaging dose, the daily CT or CBCT image-guided are still required and the target and plan isocenter alignments need to be reviewed and approved by the attending physician before the treatment delivery.

For case #5, the tumor was in a medial location in the abdomen, making it more susceptible to range uncertainties; in addition, the tumor was adjacent to the duodenum and stomach, which would influence the dose distribution owing to differences in shape and filling of these organs. These anatomical changes depend on the beam configuration, as the beam angles determine which organs are crossed by the proton paths. Organs that are subject to day-to-day variations will, if crossed, result in a less robust plan. Also, the number of fields influences the robustness, as an additional field equates to more distributed proton trajectories, which make the plan less sensitive to occasional anatomical changes. Because the inter-fraction anatomical changes cannot be estimated prior to acquiring the setup images, we suggest selecting the beam angle to avoid passing through the cavity organs first and then applying 7 or more fields to optimize the IMPT plan; especially for cholangiocarcinomas, the influences of the inter-fraction anatomical changes (such as intrahepatic deformation) might be blurred and reduced.

The deliver time required for IMPT BH treatment is an important factor to consider in the clinical implementation of the technique, as prolonged treatment time could affect patients' BH capability. Usually the patients with normal pulmonary function could hold their breath for about 20–30 s. As mention above, FGBH IMRT treatment each field could usually be delivered in 1–2 BH, so an 8 fields IMRT plan (7–11 beams for plans in this study) usually requires 8–16 BHs. For IMPT, the beam on time for each field with our current delivery system is about 60–150 s, depends on tumor size. Generally, 2 or 3 FGBHs per beam are enough for smaller tumor size and 3 or more FGBHs per beam for the large tumor size

(such as case #9). Therefore, 8–16 BHs may also be needed to deliver a 4-field IMPT plan, whereas for 7 fields plan the number of BHs needed may be doubled. We are in the process of acquiring a new delivery system with improved imaging and delivery capabilities including multiple energy extraction [33], which could result in 35% reduction of delivery time on average, and could bring the number of BHs comparable to FGBH IMRT delivery even for a 7 field plan.

There are some limitations to this study. First, the IMPT plans showed worse CI than the IMRT plans. This may due to two reasons. First, in order to keep the plan robustness, we used robust optimization for all IMPT plans, which may deliver high dose to the adjunct liver tissues to keep the plan robust for setup and range uncertainties. Second, we normalized IMPT plans for full coverage of targets ($D_{99.99\%}$ of prescribed dose) to keep the target coverage for all possible inter-fraction uncertainties, this may also lead to the dose overflow to the adjunct liver tissues. However, even with some adjunct liver tissues covered by the prescribed dose, the IMPT plans still could achieve better normal liver sparing than the IMRT plans.

Second, 4D dose calculation and rescanning strategies were not applied in this study. The IMPT is more susceptive to motion induced errors than the IMRT, so 4D dose calculation is recommended in the proton dose calculation. In this study, the FGBH beam-on window size was set to 3 mm based on external surrogate, and the residual motion within the same BH is mild [25]. The interplay between respiratory motion and spot scanning sequence is considered not obvious with the small residual motion [23]. Therefore, we did not think it was necessary to use 4D dose calculation; instead, we used the WET based beam angle selection technique to reduce the possible impact of any residual motion. The rescanning strategy in IMPT could further reduce the dose uncertainty, but its improvement may not be obvious due to the mild residual motion in the gating window; furthermore, it will prolong the delivery time [17,18]. Real time imaging and gating technique could help understand the magnitude residual motion in BH proton delivery [34].

In summary, IMPT with FGBH and CT-on-rail guidance was found to be a robust treatment approach for liver tumors. Some reductions in dose coverage of the target were observed as an effect of inter-fractional anatomical changes, such as gastrointestinal filling or liver deformation. In these cases, the IMPT plan could be improved by applying 7 or more fields to account for the change.

Acknowledgments

The University of Texas MD Anderson Cancer Center is supported in part by the National Institutes of Health through Cancer Center Support Grant P30CA016672. We thank the Department of Scientific Publications at The University of Texas MD Anderson Cancer Center for editing assistance.

Conflict of interest

None.

References

[1] Bush DA, Kayali Z, Grove R, Slater JD. The safety and efficacy of high-dose proton beam radiotherapy for hepatocellular carcinoma: a phase 2 prospective trial. Cancer 2011;117:3053–9.
[2] Hong TS, Wo JY, Yeap BY, et al. Multi-institutional phase II study of high-dose hypofractionated proton beam therapy in patients with localized, unresectable hepatocellular carcinoma and intrahepatic cholangiocarcinoma. J Clin Oncol 2016;34:460–8.
[3] Case RB, Moseley DJ, Sonke JJ, et al. Interfraction and intrafraction changes in amplitude of breathing motion in stereotactic liver radiotherapy. Int J Radiat Oncol Biol Phys 2010;77:918–25.
[4] Eccles C, Brock KK, Bissonnette J-P, Hawkins M, Dawson LA. Reproducibility of liver position using active breathing coordinator for liver cancer radiotherapy. Int J Radiat Oncol Biol Phys 2006;64:751–9.
[5] Crane CH, Koay EJ. Solutions that enable ablative radiotherapy for large liver tumors: fractionated dose painting, simultaneous integrated protection, motion management, and computed tomography image guidance. Cancer 2016;122:1974–86.
[6] Eccles CL, Dawson LA, Moseley JL, Brock KK. Interfraction liver shape variability and impact on GTV position during liver stereotactic radiotherapy using abdominal compression. Int J Radiat Oncol Biol Phys 2011;80:938–46.
[7] Crane CH. Hypofractionated ablative radiotherapy for locally advanced pancreatic cancer. J Radiat Res 2016;57:i53–7.
[8] Houweling AC, Fukata K, Kubota Y, et al. The impact of interfractional anatomical changes on the accumulated dose in carbon ion therapy of pancreatic cancer patients. Radiother Oncol 2016;119:319–25.
[9] Batista V, Richter D, Chaudhri N, et al. Significance of intra-fractional motion for pancreatic patients treated with charged particles. Radiat Oncol 2018;13:120.
[10] Lin L, Souris K, Kang M, et al. Evaluation of motion mitigation using abdominal compression in the clinical implementation of pencil beam scanning proton therapy of liver tumors. Med Phys 2017;44:703–12.
[11] Xu Q, Hanna G, Grimm J, Quantifying, et al. Rigid and nonrigid motion of liver tumors during stereotactic body radiation therapy. Int J Radiat Oncol Biol Phys 2014;90:94–101.
[12] Yang Z-Y, Chang Y, Liu H-Y, Liu G, Li Q. Target margin design for real-time lung tumor tracking stereotactic body radiation therapy using CyberKnife Xsight Lung Tracking System. Sci Rep 2017;7:10826.
[13] Worm ES, Høyer M, Fledelius W, Poulsen PR. Three-dimensional, time-resolved, intrafraction motion monitoring throughout stereotactic liver radiation therapy on a conventional linear accelerator. Int J Radiat Oncol Biol Phys 2012;86:190–7.
[14] Wurm RE, Gum F, Erbel S, et al. Image guided respiratory gated hypofractionated Stereotactic Body Radiation Therapy (H-SBRT) for liver and lung tumors: Initial experience. Acta Oncol 2006;45:881–9.
[15] Duggan DM, Ding GX, Coffey II CW, et al. Deep-inspiration breath-hold kilovoltage cone-beam CT for setup of stereotactic body radiation therapy for lung tumors: Initial experience. Lung Cancer 2007;56:77–88.
[16] Yu J, Zhang X, Liao L, et al. Motion-robust intensity-modulated proton therapy for distal esophageal cancer. Med Phys 2016;43:1111–8.
[17] Zhang Y, Knopf A-C, Weber DC, Lomax AJ. Improving 4D plan quality for PBS-based liver tumour treatments by combining online image guided beam gating with rescanning. Phys Med Biol 2015;60:8141.
[18] Zhang Y, Huth I, Weber DC, Lomax AJ. A statistical comparison of motion mitigation performances and robustness of various pencil beam scanned proton systems for liver tumour treatments. Radiother Oncol 2018;128(1):182–8.
[19] Li H, Zhang X, Park P, et al. Robust optimization in intensity-modulated proton therapy to account for anatomy changes in lung cancer patients. Radiother Oncol 2015;114:367–72.
[20] Kang Y, Zhang X, Chang JY, et al. 4D Proton treatment planning strategy for mobile lung tumors. Int J Radiat Oncol Biol Phys 2007;67:906–14.
[21] Wang X, Li H, Zhu XR, et al. Multiple-CT optimization of intensity-modulated proton therapy: Is it possible to eliminate adaptive planning?. Radiother Oncol 2018;128(1):167–73.
[22] Smith A, Gillin M, Bues M, The MD, et al. Anderson proton therapy system. Med Phys 2009;36:4068–83.
[23] Li Y, Kardar L, Li X, et al. On the interplay effects with proton scanning beams in stage III lung cancer. Med Phys 2014;41:021721.
[24] Court L, Rosen I, Mohan R, Dong L. Evaluation of mechanical precision and alignment uncertainties for an integrated CT/LINAC system. Med Phys 2003;30:1198–210.
[25] Peng Y, Vedam S, Chang JY, et al. Implementation of feedback-guided voluntary breath-hold gating for cone beam CT-based stereotactic body radiotherapy. Int J Radiat Oncol Biol Phys 2011;80:909–17.
[26] Li Y, Niemela P, Liao L, et al. Selective robust optimization: a new intensity-modulated proton therapy optimization strategy. Med Phys 2015;42:4840–7.
[27] Velec M, Moseley JL, Craig T, Dawson LA, Brock. KK. Accumulated dose in liver stereotactic body radiotherapy: positioning, breathing, and deformation effects. Int J Radiat Oncol Biol Phys 2012;83:1132–40.
[28] Brock KK, Mutic S, McNutt TR, Li H, Kessler ML. Use of image registration and fusion algorithms and techniques in radiotherapy: Report of the AAPM Radiation Therapy Committee Task Group No. 132. 2017.
[29] Cazoulat G, Owen D Fau - Matuszak MM, Matuszak Mm Fau - Balter JM, Balter Jm Fau - Brock KK, Brock KK. Biomechanical deformable image registration of longitudinal lung CT images using vessel information.
[30] Kandula S, Zhu X, Garden AS, et al. Spot-scanning beam proton therapy vs intensity-modulated radiation therapy for ipsilateral head and neck malignancies: a treatment planning comparison. Med Dosim 2013;38:390–4.
[31] International Commission on Radiation Units Measurements Report 83: Prescribing, recording, and reporting photon-beam intensity-modulated radiation therapy (IMRT). Journal of the ICRU2010.

[32] Berger T, Petersen JBB, Lindegaard JC, Fokdal LU, Tanderup K. Impact of bowel gas and body outline variations on total accumulated dose with intensity-modulated proton therapy in locally advanced cervical cancer patients. Acta Oncol 2017;56:1472–8.
[33] Younkin JE, Bues M, Sio TT, et al. Multiple energy extraction reduces beam delivery time for a synchrotron-based proton spot-scanning system. Adv Radiat Oncol. 2018;3:412–20.
[34] Shimizu S, Miyamoto N, Matsuura T, et al. A proton beam therapy system dedicated to spot-scanning increases accuracy with moving tumors by real-time imaging and gating and reduces equipment size. PLoS ONE 2014;9:e94971.